The Bacterial Cell Envelope as Delimiter of Anti-Infective Bioavailability – An *In Vitro* Permeation Model of the Gram-Negative Bacterial Inner Membrane

Florian Graef[a], Branko Vukosavljevic[a], Jean-Philippe Michel[b], Marius Wirth[c], Oliver Ries[c], Chiara De Rossi[a], Maike Windbergs[a], Véronique Rosilio[b], Christian Ducho[c], Sarah Gordon[a]* and Claus-Michael Lehr[a,d]*

[a] Helmholtz Institute for Pharmaceutical Research Saarland (HIPS), Helmholtz Center for Infection Research (HZI), Department of Drug Delivery, Campus E8 1, 66123 Saarbrücken, Germany
E-mail: Florian.Graef@hemholtz-hzi.de, Branko.Vukosavljevic@helmholtz-hzi.de, Maike.Windbergs@helmholtz-hzi.de, Chiara.DeRossi@helmholtz-hzi.de, Sarah.Gordon@helmholtz-hzi.de, Claus-Michael.Lehr@helmholtz-hzi.de
[b] Institut Galien Paris Sud, UMR 8612, Univ Paris-Sud, CNRS, Université Paris-Saclay, 5 rue J.B. Clément, F-92290 Châtenay-Malabry, France
E-Mail: jean-philippe.michel@u-psud.fr, veronique.rosilio@u-psud.fr
[c] Saarland University, Department of Pharmacy, Pharmaceutical and Medicinal Chemistry, Campus C2 3, 66123 Saarbrücken, Germany
E-Mail: marius.wirth@uni-saaland.de, christian.ducho@uni-saarland.de
[d] Saarland University, Department of Pharmacy, Biopharmacy and Pharmaceutical Technology, Campus E8 1, 66123 Saarbrücken, Germany
* Corresponding authors

Abstract

Gram-negative bacteria possess a unique and complex cell envelope, composed of an inner and outer membrane separated by an intermediate cell wall-containing periplasm. This tripartite structure acts intrinsically as a significant biological barrier, often limiting the permeation of anti-infectives, and so preventing such drugs from reaching their target. Furthermore, identification of the specific permeation-limiting envelope component proves difficult in the case of many anti-infectives, due to the challenges associated with isolation of individual cell envelope structures in bacterial culture. The development of an *in vitro* permeation model of the Gram-negative inner membrane, prepared by repeated coating of physiologically-relevant phospholipids on Transwell® filter inserts, is therefore reported, as a first step in the development of an overall cell envelope model. Characterization and permeability investigations of model compounds as well as anti-infectives confirmed the

suitability of the model for quantitative and kinetically-resolved permeability assessment, and additionally confirmed the importance of employing bacteria-specific base materials for more accurate mimicking of the inner membrane lipid composition - both advantages compared to the majority of existing *in vitro* approaches. Additional incorporation of further elements of the Gram-negative bacterial cell envelope could ultimately facilitate model application as a screening tool in anti-infective drug discovery or formulation development.

Keywords: Gram-negative bacterial cell envelope, permeation kinetics, permeability investigations, *in vitro* permeation model

CL	cardiolipin
ER	electrical resistance
IM	inner membrane
KRB	Krebs-Ringer buffer
LC	liquid condensed
LE	liquid expanded
MIC	minimal inhibitory concentration
OM	outer membrane
PC	phosphatidylcholine
PL	phospholipid
P_{app}	apparent permeability coefficient
PBS	phosphate buffered saline
PMB	polymyxin B
POPE	1-hexadecanoyl-2-(9*Z*-octadecenoyl)-*sn*-glycero-3-phosphoethanolamine
POPG	1-hexadecanoyl-2-(9*Z*-octadecenoyl)-*sn*-glycero-3-phospho-(1'-*rac*-glycerol)

PVPA	phospholipid vesicle-based permeation assay
SE	standard error of the mean
SEM	scanning electron microscopy
UHPLC	ultra-high performance liquid chromatography

1. Introduction

The increasingly reported occurrence of multidrug-resistant bacteria, particularly those of the Gram-negative classification, constitutes a growing threat to the state of health worldwide [1,2]. The up-regulation and evolution of bacterial resistance mechanisms, leading to inadequate drug levels at target sites, in fact acts to exacerbate the already challenging task of successfully delivering anti-infective compounds or formulations into or across the cell envelope [3]. The unique and complex structure of the Gram-negative bacterial envelope operates intrinsically as a significant barrier, preventing the attainment of sufficient drug levels at required sites of action in many instances [4,5]. The envelope itself consists of an inner membrane (IM) of phosphatidylethanolamine, phosphatidylglycerol and cardiolipin as principal phospholipid (PL) components, together with an asymmetric outer membrane (OM) composed of a PL-containing inner leaflet and a lipopolysaccharide-containing outer leaflet. These two membrane structures, additionally incorporating aspects of active transport, are chiefly responsible for the intrinsic barrier properties of the envelope, which is therefore commonly termed as a two-membrane barrier [6]. In addition however, the periplasmic space separating the IM and OM serves as an area of high metabolic activity [7], and also houses the peptidoglycan cell wall (a much thinner structure in comparison to Gram-positive bacteria). The described intrinsic and resistance-compounded difficulties in achieving adequate drug levels at bacterial target sites, together with the present low flow within the antibiotic development pipeline, both contribute to a common inability to successfully treat Gram-negative bacterial infections. Such difficulties can ultimately and collectively be regarded as symptoms of a bacterial bioavailability problem [8], which is of vital importance to address. The development of new anti-infective compound classes, the discovery of new targets, and the advent of novel delivery strategies which facilitate effective anti-infective drug penetration into or completely across the cell envelope (in order to reach intracellular sites of

action) therefore all constitute important areas of research in this respect. In addition, research efforts within these areas require an increased understanding of and ability to investigate bacterial permeation processes - a difficult task to achieve currently *in cellulo* due to numerous associated challenges [8]. As such, a further research need to be addressed is the requirement for models which allow for the characterization and quantification of anti-infective permeation across the Gram-negative bacterial cell envelope. Such models would provide complementary information to that obtained from established, '*in cellulo*' efficacy testing approaches (such as determination of minimum inhibitory concentrations (MIC)), allowing for optimization of drug candidates with respect to their target interaction as well as their ability to sufficiently permeate the envelope barrier [9].

A variety of *in vitro* models in fact already exist for investigating interactions between anti-infective compounds and bacterial cell envelope components; these can generally be classified as electrophysiology models [10,11], Langmuir films [12] and vesicle-based assays [13]. While all such models are able to provide insight into bacterial permeation processes, they also demonstrate several shortcomings. For instance, most focus on approximating the IM or the OM alone, rather than both structures together (although some progress in this respect has been recently made [14]). Furthermore, the PL composition of existing IM models often deviates from that found in Gram-negative bacteria, in terms of either character or ratio [15]. The majority of the available approaches also do not allow for the quantification of permeation processes [14, 16-18], an important ability which would allow for more in-depth and accurate characterization of the way in which anti-infective compounds and formulations interact with the bacterial envelope barrier [19]. Hence, there is a great need for new models which represent the entire Gram-negative bacterial envelope with respect to both composition and structure, and which are specifically designed to yield high content, quantitative permeation information in a kinetically- and ultimately spatially-resolved manner.

As a first step in the production of an overall envelope model, this work is aimed at designing and characterizing an *in vitro* model of the Gram-negative bacterial IM employing bacteria-specific PLs, which is explicitly designed to quantify the passive permeation kinetics of anti-infectives. A Transwell®-based setup, mimicking the conventional procedure to assess permeation through mammalian cell barriers, was employed for the model preparation process. An existing approach for production of lipid-based mammalian membrane models – the phospholipid-vesicle based permeation assay (PVPA) [20] - was adapted in order to prepare the bacterial IM model, utilizing a bacteria-specific lipid composition as found in the IM of Gram-negative bacteria such as *Escherichia coli* and *Pseudomonas aeruginosa* [21]. The resulting preparation procedure was also employed to produce a model consisting solely of phosphatidylcholine, as a major phospholipid in mammalian cell membranes [20]. The IM model and the phosphatidylcholine-containing mammalian model ('mammalian comparator') were then directly compared at each stage of IM characterization and in subsequent permeability studies. This comparison was made in order to discern any lipid-dependent differences between the models in terms of structure and function, and in doing so, to clearly demonstrate the need to adapt an already existing mammalian lipid-based model using bacteria-relevant materials. Models were characterized with respect to the interfacial behavior of their component lipids, as well as integrity and robustness, topography, and thickness. Furthermore, sets of model compounds including anti-infectives were utilized to ultimately assess the impact of model lipid composition on permeability behavior, and to highlight the ability to obtain quantitative and kinetically-resolved permeation data.

2. Material and methods

2.1. Materials

1-hexadecanoyl-2-(9*Z*-octadecenoyl)-*sn*-glycero-3-phosphoethanolamine (POPE), 1-hexadecanoyl-2-(9*Z*-octadecenoyl)-*sn*-glycero-3-phospho-(1'-*rac*-glycerol) (sodium salt) (POPG) and 1,1',2,2'-tetra-(9*Z*-octadecenoyl) cardiolipin (sodium salt) (CL) purchased from Avanti Polar Lipids Inc. (Alabaster, AL, USA) were used for the IM model preparation. Egg phosphatidylcholine (PC, Lipoid E80) was kindly donated by Lipoid GmbH (Ludwigshafen, Germany), and employed for the mammalian comparator model. Polycarbonate filters with a pore size of 800 nm (Merck Millipore, Darmstadt, Germany) were used for liposome extrusion. Commercially available cell culture inserts (Transwell® permeable supports 3460) were obtained from Corning Inc. (Acton, MA, USA). Calcein, sodium fluorescein, rhodamine 123, rhodamine B, rhodamine B isothiocyanate, atenolol, metoprolol tartrate, timolol maleate, nadolol, acebutolol hydrochloride and alprenolol hydrochloride (Sigma-Aldrich Co., St. Louis, MO, USA) served as model drugs. Polymyxin B (PMB), minocycline hydrochloride and ciprofloxacin hydrochloride (Sigma-Aldrich Co., St. Louis, MO, USA) were employed as anti-infective agents. All reagents for ultra-high performance liquid chromatography (UHPLC) were purchased from VWR (Radnor, PA, USA). All other chemicals and solvents were of at least analytical grade.

2.2 Methods

2.2.1 Langmuir trough experiments

Surface pressure-area π-A measurements of lipid monolayers composed of pure bacteria-relevant PLs (POPE, POPG, CL), their 70:20:10 weight mixture [21], or pure PC were performed using a thermostated Langmuir film trough (775.75 cm^2, Biolin Scientific, Finland) enclosed in a plexiglas box. Experiments were performed at 294 and 303 K (21±1 °C and 30±1 °C respectively). PLs were dissolved in a mixture of chloroform and methanol (9:1 v/v) to form solutions of 1 x 10^{15} molecules/µl. These solutions were then used to spread PLs at

the air/buffer interface, following subphase cleaning by suction. After PL deposition, the system was left for 15 min to allow complete evaporation of the organic solvents. Monolayer compression was then performed at a speed of 5 $Å^2$ *molecule^{-1} *min^{-1}. The results reported are mean values of at least two measurements. The surface compressional moduli (K) of monolayers were calculated from equation (1):

$$K = -A*\left(\frac{d\pi}{dA}\right) \quad (1)$$

where A is the PL molecular area ($Å^2$), dπ the surface pressure change (mN/m) and dA is the change in the molecular area.

2.2.2 Model preparation

Both the bacterial IM and the mammalian comparator model were produced by adapting the PVPA approach [20]. Liposomes composed of bacteria- or mammal-relevant PLs were first prepared via the lipid film hydration method [22]. Briefly, POPE, POPG and CL were used in a 70:20:10 weight ratio, as a bacteria-specific PL mixture. PC was used as mammal-specific PL. POPE, POPG and CL, or PC alone were dissolved in a mixture of chloroform and methanol (3:1, 5 ml) in a round-bottom flask (250 ml). Organic solvents were then removed under reduced pressure (1 h: 200 mbar, 30 min: 40 mbar; 70 °C (bacteria-specific PL mixture); 55 °C (mammal-specific PL)) using a Rotavapor R-205 (BÜCHI Labortechnik GmbH, Essen, Germany) in order to form a thin lipid film. Phosphate buffered saline (PBS; adjusted to pH 7.4) containing ethanol (10% v/v) was used to rehydrate the lipid film to obtain the liposome dispersions (6% w/v total lipids). Afterwards, liposomes were sonicated for 1 h and subsequently extruded (10 times; at 70 °C in case of the bacteria-relevant liposomes and 55 °C in case of the mammal-relevant liposomes), using a Liposofast L-50 extruder (Avestin

Europe GmbH, Mannheim, Germany). Both IM and mammalian comparator models were then prepared by three consecutive cycles of liposome addition (75 µl each) onto filter supports, followed by centrifugation (30 min, 1040 g; Hettich Rotina 420 R, Hettich GmbH, Tuttlingen, Germany) and oven-drying (50 min, 50 °C), with a final freeze-thaw step (-80 °C, 20 min; 45 °C for 20 min).

2.2.3 Liposome size and surface charge measurements

The hydrodynamic diameter and size distribution of liposomes was measured in PBS (adjusted to pH 7.4) using dynamic light scattering, while surface charge (ζ-potential) was determined (in the same medium) using laser doppler micro-electrophoresis (Zetasizer Nano ZS, Malvern Instruments, UK).

2.2.4 Confocal Raman microscopy

Confocal Raman microscopy analysis was carried out to investigate the integrity of IM and mammalian comparator model lipid coatings using a WITec alpha 300R+ imaging system (WITec GmbH, Ulm, Germany), with an Olympus 50 x objective (N.A. 0.35). The excitation source was a diode laser with a wavelength of 785 nm (50 mW). Models were analyzed following preparation, and after 5 h incubation in Krebs-Ringer buffer (KRB) at 37 °C without any further sample alteration. A confocal pinhole of 100 µm rejected signals from out-of-focus regions. Raman spectra were acquired every 100 µm along the x- and y-axis across the entire model membrane area, with an integration time of 4 s. Cosmic ray removal and background subtraction were applied to all spectra, which were then processed using hierarchical cluster analysis and basis analysis as multivariate methods for data processing, and converted into spatially-resolved false-color images using WITec Project Plus software (WITec GmbH, Ulm, Germany).

2.2.5. Laser scanning interferometry

Model topography was analyzed via a LEXT OLS4000 3D Laser Measuring Microscope (Olympus AG, Tokyo, Japan), using a 405 nm semiconductor laser and a 20 x objective lens. Transwell® membranes with PL coatings were cut out of the plastic Transwell® holder surround and fixed on sample holders. Five representative membrane areas with an image size of approximately 5.6 mm^2 each were analyzed. The center of the overall model surface was denoted as area 1. The center of further imaged edge areas was set at a distance of 3000 µm from the upper (2), right (3), bottom (4) and left (5) margin of the overall membrane surface.

2.2.6 Scanning electron microscopy

For scanning electron microscopy (SEM) investigations, freshly prepared model membranes were first freeze-dried (Christ alpha 2-4 plus, Martin Christ Gefriertrocknungsanlagen GmbH, Osterode am Harz, Germany). As for laser scanning interferometry, Transwell® membranes with PL coatings were then cut out of the plastic holder surround; filter membranes were subsequently removed. Vertical cross-sections of model membranes prepared using a scalpel were then sputtered with gold, placed in a vertical manner on sample grids and subsequently analyzed via SEM (Zeiss EVO HD 15, Carl Zeiss AG, Oberkochen, Germany).

2.2.7. Permeability investigations

For investigation of permeability behavior, transport studies were performed with at least 6 repetitions from 2 individual experiments. IM and mammalian comparator model-permeated amounts of fluorescent dyes and ß-blockers were determined, as model compounds. Amounts of permeated ciprofloxacin and minocycline (with and without 1 h of model pre-incubation with 15.4 µM PMB), as well as an AlexaFluor® 488-labeled functionalized fatty acid moiety of the muraymycin A series of nucleoside antibiotics, together with corresponding reference

compound (both synthesized in-house according to Ries *et* al. [23]), were determined as anti-infective substances.

Prepared model membranes on Transwell® filter inserts were placed in cell culture plates and pre-incubated to rehydrate and equilibrate the system with pre-warmed KRB (pH 7.4, 37 °C) for 30 min (upon which electrical resistance (ER) values were seen to stabilize, see Supplementary Material). Following KRB removal, 520 µl of drug solution in KRB, in each case at a concentration calculated in order to ensure sink conditions and adjusted to pH 7.4 (see Supplementary Material Tables S1 and S2, 1.27 µM in case of the functionalized fatty acid moiety and reference compound) was added to the apical compartment of each culture plate well (donor). A 1.5 ml volume of pre-warmed KRB was also added to the basolateral compartment (acceptor). A 20 µl volume of drug solution in KRB was immediately removed from the apical compartment, and employed to accurately measure the starting donor concentration. Samples of 200 µl were taken from the basolateral compartment of culture plate wells after 0, 0.5, 1, 1.5, 2, 2.5, 3.5 and 4.5 h, and used to quantify the permeated amount of applied compounds (see below). The removed volume was replaced with an equal volume of pre-warmed KRB in order to maintain sink conditions. Cell culture plates containing coated Transwell® filter inserts were placed on an orbital shaker (IKA®-Werke GmbH and Co KG, Staufen, Germany) set at 150 rpm and kept at 37 °C in an incubator for the duration of transport studies.

2.2.8. Quantification of permeated compound/drug amount and permeability calculations

A Tecan Infinite® M200 plate reader (Tecan GmbH, Crailsheim, Germany) was used to determine the permeated amount of fluorescent dyes (see Supplementary Material Table S1). A Dionex Ultimate® 3000 UHPLC with an Accucore column (RP 18, 150 mm x 2.1 mm, 2.6 µm, Thermo Fisher Scientific Co., Waltham, MA, USA) was used to quantify the permeated

amount of ß-blockers, ciprofloxacin and minocycline in transport studies. ß-blocker quantification was carried out using a binary solvent system (A = 36.6 mM Na_2HPO_4 + 33.4 mM triethylamine adjusted to pH 3; B = acetonitrile) as eluent in different ratios, depending on the analyte; the flow rate and resulting compound retention time also varied (see Supplementary Material Table S2). The column oven temperature in all cases was set to 40 °C. Ciprofloxacin and minocycline quantification was also carried out using a binary solvent system (A= 0.02 M Na_2HPO_4 adjusted to pH 2.7; B= acetonitrile) as eluent in different ratios. The resulting retention time also varied (see Supplementary Material Table S2). The column oven temperature was set to 25 °C for ciprofloxacin and to 40 °C for minocycline. Permeated amounts of AlexaFluor® 488-labeled fatty acid moiety and corresponding reference compound were determined as described above for fluorescent dyes, with $\lambda_{exc.}$ (nm) = 470 and $\lambda_{em.}$ (nm) = 520.

In all cases, the permeated compound amount was calculated in reference to calibration curves created from samples of standard concentration. The cumulative permeated compound amount was then plotted as a function of time. The slope of the linear region of this curve constitutes the rate of compound flux, which was used to calculate the apparent permeability coefficient (P_{app}) of each compound according to equation (2):

$$P_{app}\ (cm/sec) = J/(A*c_0) \qquad (2)$$

where J is the substance flux (mg/sec), A the surface area of the Transwell® filter insert (cm^2) and c_0 the initial compound concentration (mg/ml).

2.2.9. Statistical analysis:

Where appropriate, presented numerical data represent mean ± standard error of the mean (SE). Student's t-test was employed where relevant to evaluate significant differences (*=*P* <

0.05, ***=P<0.001). All tests were calculated using the software SigmaPlot version 12.5 (Systat Software, Inc., San Jose, California, USA).

3. Results and discussion

3.1. Bacterial IM and mammalian comparator membrane model preparation, characterization and comparison

3.1.1. Interfacial behavior comparison of bacteria- and mammal-relevant phospholipids

Prior to IM model development and optimization the interfacial behavior of individual bacterial PLs, a bacterial PL mixture, and the mammal-specific PC was characterized using the Langmuir trough technique. Surface pressure-area measurements of pure POPE, POPG and CL monolayers were carried out, as well as the ternary mixture of POPE:POPG:CL in a relevant 70:20:10 weight ratio were carried out to confirm miscibility of the bacterial PL components. Investigation of PC lipid monolayers was also carried out in order to investigate the occurrence of any notable differences in behavior of PC and the bacterial PL mixture at the molecular level. Surface pressure-area isotherms were initially obtained at 21 °C, followed by the more physiologically relevant temperature of 30 °C (representing the highest temperature that could be applied in the experimental setup without the introduction of inaccuracies caused by buffer evaporation) (Fig. 1A). Isotherms were then used to calculate the compressibility moduli of PL monolayers (Fig. 1B).

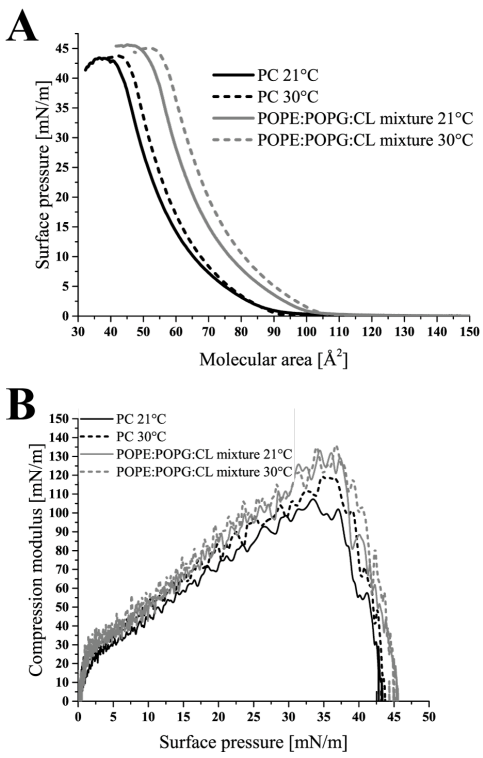

Fig. 1. Langmuir studies of bacterial IM and mammal-relevant PLs. Compression isotherms for bacteria-specific PL mixture (POPE:POPG:CL) and pure PC monolayers at 21 °C and 30 °C (A), showing differences in two-dimensional organization. Corresponding compressibility moduli as a function of surface pressure for both tested monolayers are additionally depicted (B), demonstrating the greater rigidity of the POPE:POPG:CL monolayer as compared to PC.

The isotherms obtained for the ternary bacterial PL mixture at 21 °C appeared to be intermediate between those of pure POPG and POPE (see Supplementary Material Fig. S1A), demonstrating that, although POPE is the major component of the ternary bacterial PL mixture, it is not the only mixture component contributing to the interfacial behavior. The influence of POPG and CL on the surface area-pressure measurements of POPE:POPG:CL monolayers, together with free energy of mixing and excess molecular area calculations (see Supplementary Material Fig. S1B, S1C) therefore implies the existence of a true lipid mixture. Comparison of the isotherms for the ternary mixture and pure PC monolayers revealed similar collapse pressures (π_c) at both 21 °C and 30 °C (Fig. 1A), with values around

44 mN/m (Table 1). However, the isotherm-derived larger molecular areas for the lipid mixture at pressure onset (A_{onset}) and collapse (A_c) account for more expanded monolayers of the ternary mixture compared to those of pure PC.

Table 1. Summary of conducted Langmuir studies. Characteristic parameters of compression isotherms, comparing the bacteria-relevant POPE:POPG:CL mixture to PC at 21 °C and 30 °C.

Applied Temperature (°C)	**Monolayer**	**A_{onset} (Å²)**	**A_c (Å²)**	**π_c (mN/m)**
21	POPE:POPG:CL	103.0	51.6	45.4
21	PC	97.5	43.5	42.9
30	POPE:POPG:CL	107.5	55.8	44.9
30	PC	92.3	45.4	43.5

A_{onset}: molecular area at pressure onset, A_c: molecular area at collapse, π_c: surface pressure at collapse

In addition to information gained directly from the isotherms, compressibility moduli were calculated in order to determine the physical state of the PC and PL mixture monolayers at various surface pressures. Compressibility moduli below 12.5 mN/m, in the range of 13-100 mN/m, from 100 to 250 mN/m and above 250 mN/m infer a gaseous, liquid expanded (LE), liquid condensed (LC) and solid state of monolayers [24], respectively. PL organization at surface pressures in the range of 25-35 mN/m is of particular interest, as this represents the pressure range considered to correspond to the internal lateral pressure found in natural membranes [25]. PC monolayers were found to be in an LE state at 21 °C within this surface

pressure range, whereas POPE:POPG:CL monolayers appeared to be in the LC state. PC monolayers were only observed to be in the LC state at higher surface pressures, from 30-38 mN/m (Fig. 1B). A similar observation was made from measurements performed at 30 °C. As a result of this interfacial analysis, the bacterial PL mixture monolayer can be regarded as being greater in molecular area and slightly more rigid compared to that of PC, at both investigated temperatures; a first indication of differences in the behavior of bacteria- and mammal-specific lipids on a molecular level can therefore be inferred.

3.1.2. Bacterial IM and mammalian membrane model preparation

Following initial Langmuir studies, membrane models consisting of the previously employed POPE:POPG:CL in a 70:20:10 weight ratio (bacterial IM model) and pure PC (mammalian comparator model) were prepared, via the PVPA approach [20]. In this two-step approach, liposomes consisting of the PLs of interest are first prepared, as a means to facilitate lipid deposition onto Transwell® filter supports without the use of organic solvents; liposomes are then repeatedly coated onto filter supports in order to form a lipid membrane structure. Although serving only as a means for lipid deposition, prepared POPE:POPG:CL and PC liposomes were analyzed in terms of their hydrodynamic diameter and surface charge (ζ-potential) in order to confirm a consistent outcome of liposome production. Low variation in z-average and surface charge of both POPE:POPG:CL and PC liposomes confirmed the acceptability of liposome preparation (see Supplementary Material Table S3), whereas differences between bacterial and mammalian lipid liposomes (for instance with respect to size) could be regarded as an outcome of the previous elucidated differences in PL packing properties (see section 3.1.1).

While PVPA models consisting of PC alone have been previously established [26-28], the primary objective of the current work was to develop a bacterial IM model. For this reason,

model preparation was adapted and optimized with respect to the use of POPE:POPG:CL. The IM-optimized preparation procedure was then applied using PC liposomes in order to produce a mammalian model which was truly comparative in nature. The procedure applied to deposit and coat liposomes on a Transwell® filter was required to result in the construction of an IM surrogate exhibiting robust permeation barrier properties, as well as a high level of stability on exposure to buffer (as would occur during transport studies). Thus, the model preparation procedure was optimized to fulfil these requirements. Deposition and coating parameters were refined by tracking the impact of parameter alterations on model barrier function in simulated transport experiments (entailing exposure to KRB, pH 7.4, 37 °C, for 5 h). Barrier properties of the IM model were inferred from measurement of ER, a common means of monitoring barrier integrity in both cell-based [29,30] as well as cell-free [20] permeation models (See Supplementary Material Figure S2).

The optimized preparation procedure (Fig. 2) consisted of three consecutive cycles of liposome addition to a Transwell® filter insert, centrifugation and drying, followed by a final freeze-thaw step – this step has been shown to promote liposome fusion, leading to a confluent PL coating (rather than layers of discrete liposomes) with stable barrier function [26]. The bacterial IM model constructed via this procedure showed sufficiently high and constant ER values throughout a 5 h period of exposure to KRB (see Supplementary Material Fig. S2), with no visible detachment of lipid coating from the Transwell® filter support. The described preparation procedure as optimized for IM model preparation was then used for preparation of a mammalian comparator model, by coating with PC liposomes. The comparator model also demonstrated a high and stable level of ER upon incubation with KRB (data not shown), as well as a lack of visible detachment from the Transwell® filter support.

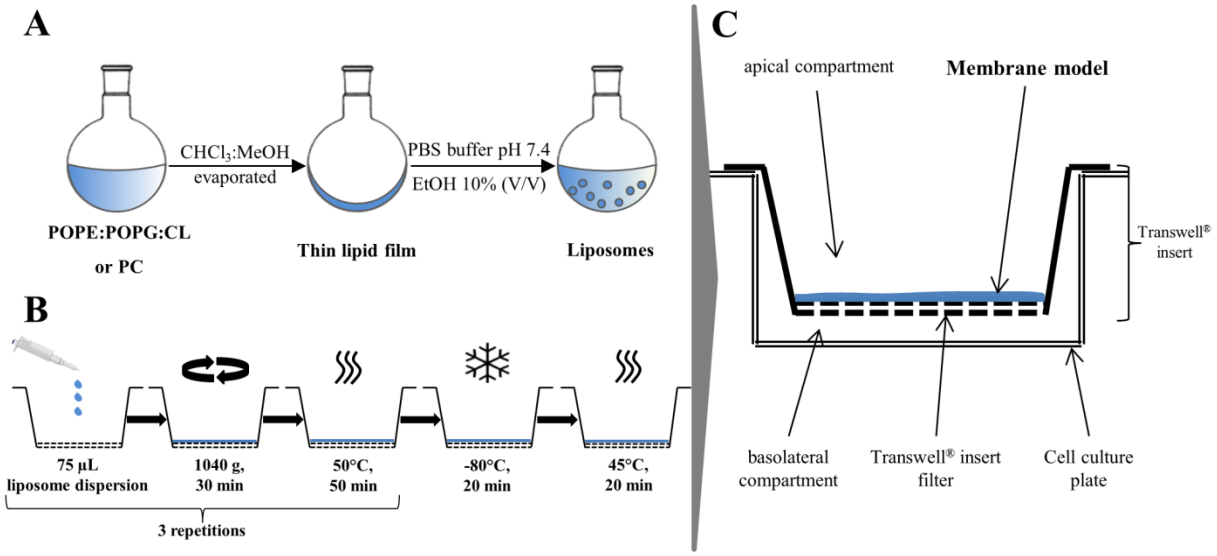

Fig. 2. Model preparation procedure. Schematic of the two-step PVPA model preparation procedure, consisting of liposome preparation (A) and subsequent coating with liposome dispersions to form IM and mammalian comparator models (B). Liposomes consisting of POPE, POPG and CL were used to construct the bacterial IM model, while PC liposomes were employed to prepare the mammalian comparator. The final set-up of a model (blue) placed on top of a Transwell® filter support is additionally shown (C).

3.1.3. Model integrity and topography assessment

As described above, the optimized preparation procedure was seen in both the case of the IM and mammalian comparator model to result in a stable and robust membrane structure with appreciable barrier function. These properties can themselves be taken as an indication of a continuous and uninterrupted coating of bacteria- or mammal-specific lipids on Transwell® filter inserts. However, as any discontinuity present initially in the membrane structure or developing during transport experiments has the potential to lead to overestimation of the permeated amount of tested compounds/drugs and so distortion of resulting permeability data, it was deemed necessary to further investigate and firmly establish model integrity. Chemically selective analysis of the entire surface area of Transwell® filter inserts accommodating either the IM or mammalian comparator model was therefore performed

using confocal Raman microscopy, to determine model integrity following preparation as well as following incubation in buffer (as described above for simulated transport studies). Due to the structured surface of the models, optical topography was applied prior to confocal Raman microscopy experiments in order to adjust the focus according to the sample topography, and to characterize topography of the overall model area. Topography profiles indicated a higher surface height at the edges compared to the center in the case of both models (see Supporting Information Figure S3). This was expected due to the model preparation procedure, and is in agreement with previous investigations [31].

Confocal Raman microscopy as such allows for label-free discrimination between the polyester material of the Transwell® filter inserts and the PLs of the membrane models, based on the individual spectra of the compounds. Consequently, the method allows for determination of the extent to which Transwell® filter inserts are covered with model PLs. Recorded Raman spectra were processed and subsequently converted into spatially-resolved false color images, in order to enable visualization of the integrity of lipid coating (Fig. 3, bacteria-relevant lipids of the IM model in blue, mammal-relevant lipids of the comparator model in green). Continuous bacterial PL coverage of Transwell® filter inserts was observed directly after IM model preparation, with no sign of coating defects (Fig. 3A); this continuous lipid coating was seen to remain entirely intact following 5 h incubation of the IM model in transport buffer (Fig. 3B). Likewise, the mammalian comparator model showed a continuous coverage and the absence of any defects in the PL layer immediately following preparation (Fig. 3C). Furthermore, no lipid-free Transwell® areas were observed following simulated transport experiments (Fig. 3D). Even though variations in Raman signal intensity translating to color intensity gradients could be observed in some images (especially Fig. 3D), overall intact PL coverage was confirmed by the presence of lipid-specific peaks over the entire Transwell® filter area in both models, before and after exposure to KRB. For illustration, the

individual raw Raman spectra derived from the central as well as from the outer region of coated filter membranes (marked by black and red crosses respectively) are presented below each of the Raman images in Fig. 3. The confirmed integrity of both the bacterial IM and mammalian comparator models, together with the earlier demonstrated appropriate and stable model barrier properties, therefore indicates the feasibility of compound permeability determination in the IM and comparison with the mammalian comparator.

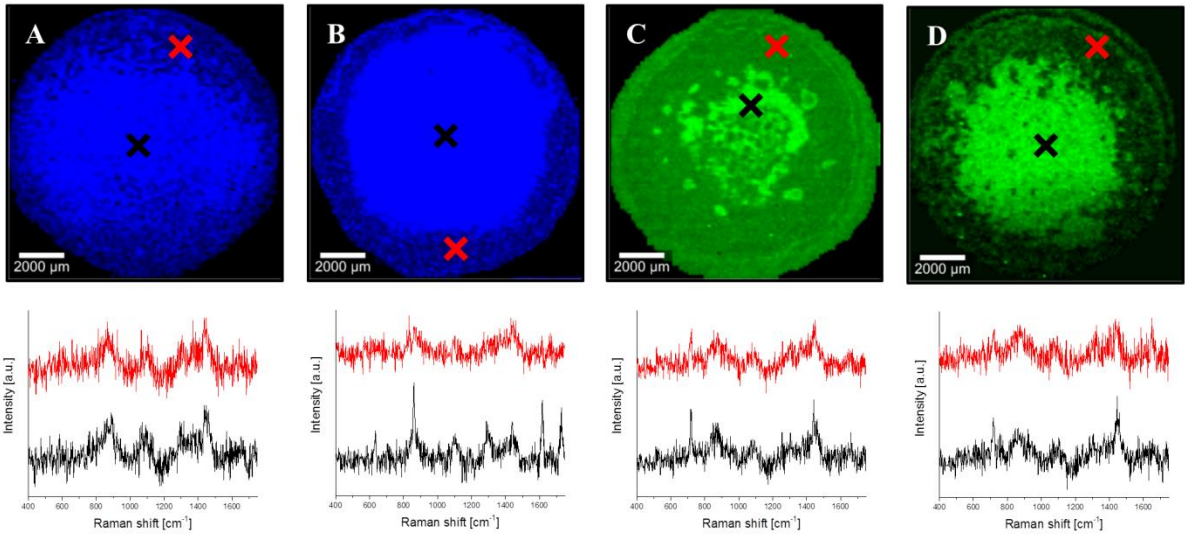

Fig. 3. Integrity assessment of the IM and mammalian comparator model. False color images with representative single Raman spectra of central and outer regions of coated Transwell® filter inserts, showing the IM model with bacteria-relevant lipids indicated in blue before (A) and after (B) exposure to KRB, as well as mammal-relevant lipids of the comparator model in green before (C) and after (D) exposure to buffer. The presence of lipid-specific Raman peaks in all single Raman spectra at 1440 cm^{-1} (in raw state without any further spectral manipulation, e.g. smoothing or subtraction) confirmed the overall lipid coverage. Color intensity differences represent the variation in Raman signal intensity, not a lesser degree of lipid coverage.

Having established that both the bacterial IM and mammalian comparator model were suitable for permeability investigations, the focus of further characterization shifted towards

comparison and contrast of model properties. Following initial optical topography investigations, laser scanning interferometry was employed to obtain more detailed insights into the topographical profiles of both the IM and mammalian comparator model following preparation. Hence, the bacterial IM model surface was analyzed at five representative positions (center; upper, right, bottom and left edges) each with an approximate image size of 5.6 mm^2, representing the maximum image size of the employed objective (Fig. 4A). A lower height maximum of approximately 73 µm, as well as a more uniform surface profile were found at the center of the IM model (Fig. 4B 1) as compared to the edge areas, which showed height maximums of up to 184 µm (Fig. 4B 2-5). The mammalian comparator model exhibited a similar contrast in surface height maximums and profile uniformity when comparing center and edge areas (Fig. 4C 1-5), indicating no marked differences in initial topography of IM and mammalian comparator models.

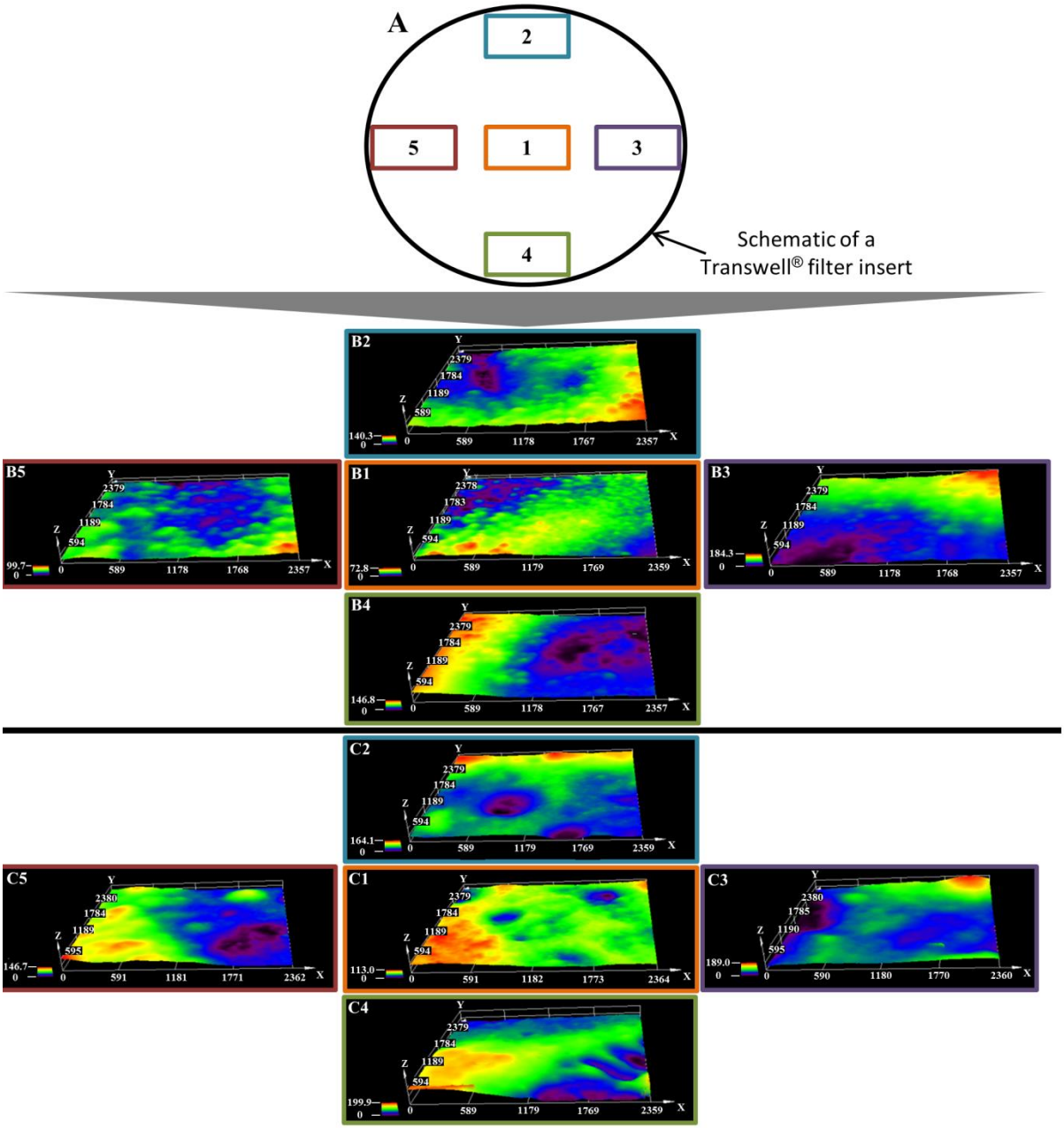

532 **Fig. 4.** Surface topography assessment of the IM and mammalian comparator model.
533 Schematic of the model surface showing the location of the representative imaged areas (A).
534 Topography of the bacterial IM model imaged at the five representative model areas (center
535 (B1), as well as upper (B2), right (B3), bottom (B4) and left (B5) edges) is shown. The same
536 areas of the mammalian comparator model (center (C1), upper (C2), right (C3), bottom (C4)
537 and left (C5) edges) were additionally imaged.

538

539

540

3.1.4. Model thickness assessment

Model thickness constitutes another parameter which potentially affects the permeability behavior of tested compounds/drugs [32]. Therefore, further to confirming model integrity and an absence of drastic differences in surface topography, it had to be ensured that the IM and the mammalian comparator model exhibited comparable values in the z dimension. Freeze-dried, vertical cross-sections of both models were therefore applied in their original orientation on sample grids and subsequently imaged and sized using SEM. Analysis of SEM images revealed similar thicknesses of the IM and the mammalian comparator model, with values of approximately 160 µm in both cases (Fig. 5). SEM images additionally indicated differences in inner model morphology, potentially occurring as a result of the differences in employed PLs; this indication was further confirmed by cryo-SEM analysis of IM and mammalian comparator models (see Supplementary Material Figure S4).

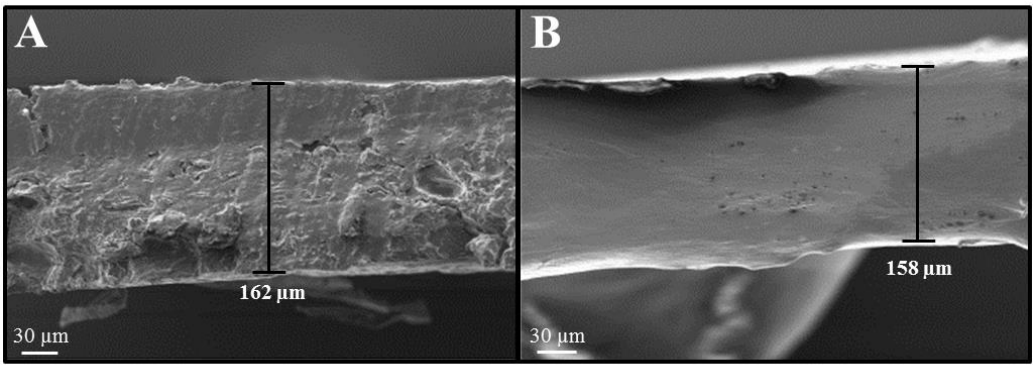

Fig. 5. Thickness evaluation of the IM and mammalian comparator model. Representative SEM images of vertical cross sections of the bacterial IM (A) and mammalian comparator model (B) without underlying Transwell® filter, indicating similarity in model thickness (Images are representative of n=3 investigations, with mean values of 156 ± 18 µm and 165 ± 6 µm for the IM and mammalian comparator model respectively).

3.2 Evaluating the impact of model lipid composition on the permeability behavior of compounds/drugs

The characterization measures employed in previous sections confirmed the suitability and robustness of the bacterial IM model for transport studies, as well as the mammalian model as a relevant comparator. Bacterial IM and mammalian comparator models prepared using the same standardized procedure showed a required similarity in properties such as thickness, yet demonstrated some degree of variation on both the molecular and microscale, as a function of the different employed PLs. Whether such PL-dependent variations translated into differences in permeability behavior in the IM and the mammalian comparator model was then further investigated, to discern the importance and necessity of producing a bacterial IM model specifically employing bacterial lipids in a physiologically relevant ratio.

A set of readily-quantifiable fluorescent dyes exhibiting a range of distribution coefficients at pH 7.4 (log $D_{(pH\ 7.4)}$) was utilized in a first step in order to conduct a preliminary proof of concept study (see Supplementary Material Table S1). Point-wise differences in P_{app} values of such compounds in the IM and the mammalian comparator were noted, showing a trend for greater compound permeation across the IM model (Fig. 6A). This was seen to occur even in case of the negatively charged dyes calcein and fluorescein, which could potentially have been predicted to interact with negatively charged PLs (such as POPG and CL of the IM) in a repulsive way, resulting in a low level of permeation [33]. Following this encouraging preliminary result, it was decided to test a set of compounds which also varied in lipophilicity, but which showed a much greater similarity with respect to other physicochemical parameters (Table 2). For this purpose β-blockers were selected, as a standard compound set frequently employed in cell- [34] and lipid-based [35,36] *in vitro* models for determination of discriminatory capabilities. Utilizing this set of compounds additionally allowed for permeability comparisons of the original PC-containing PVPA model with the current

mammalian comparator, further confirming its appropriateness to serve as a reference model in the current work (see Supplementary Material Figure S5).

Table 2. Important physicochemical parameters of employed ß-blockers.

ß-blocker	log $D_{(pH\ 7.4)}$[a)]	M_w (g/mol)	PSA (A^2)[b)]	H-bond donors/acceptors[b)]
Atenolol	-1.29	266.3	94.6	3 / 4
Metoprolol	-0.16	267.4	58.4	2 / 4
Timolol	0.03	316.4	85.2	2 / 8
Nadolol	0.68	309.4	88.8	4 / 5
Acebutolol	0.83	336.4	92.8	3 / 5
Alprenolol	1.38	249.3	43.7	2 / 3

PSA: polar surface Area
[a)] Values from Zhu *et al*.[37])
[b)] Values from Pubchem

Pair-wise comparisons of β-blocker permeability data again revealed significant point-wise differences in P_{app} values (Fig. 6B), with a higher degree of permeation noted in the case of the IM model in contrast to the mammalian comparator across the entire tested range of compound lipophilicities. This observation further confirms the impact of model lipid composition on compound permeability behavior.

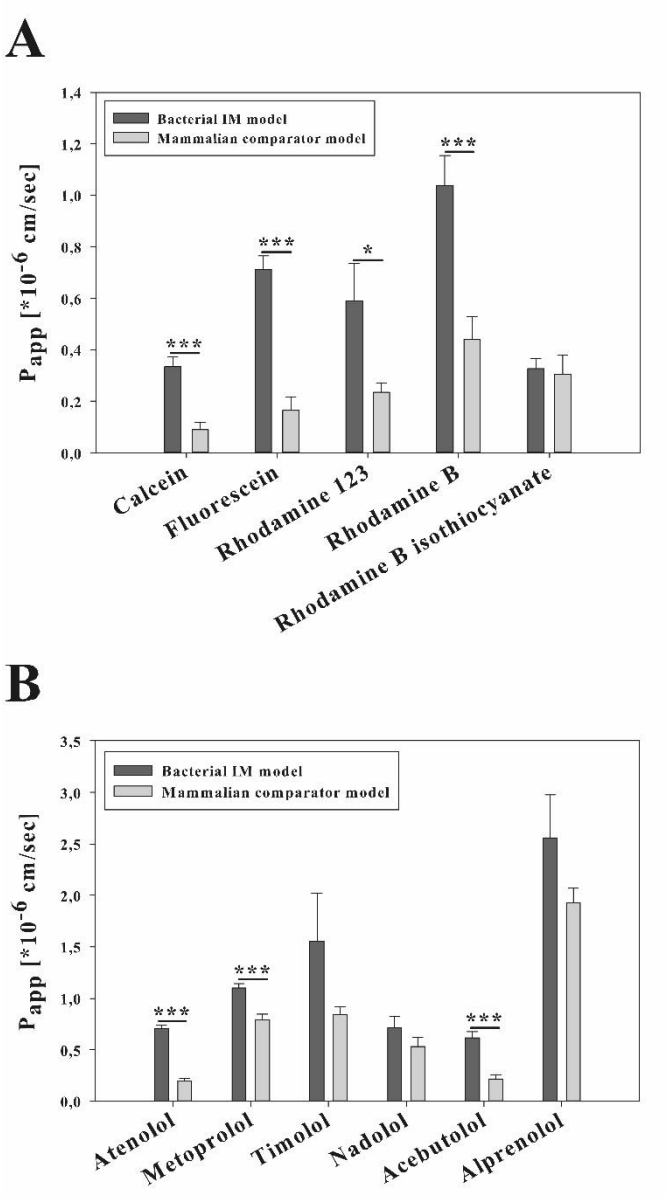

Fig. 6. Permeability experiment results of model compounds. P_{app} values of fluorescent dyes (A) and ß-blockers (B), both in order of increasing lipophilicity, in the bacterial IM and mammalian comparator model. Values represent mean ± SE; n≥9 from 3 individual experiments; *=P<0.05, ***=P<0.001.

3.3 Permeation and interaction of anti-infectives with the IM model in comparison to the mammalian comparator model

The assessment and comparison of model compound permeability in the IM and mammalian comparator model demonstrated an impact of the PL composition on compound permeation. It was then further investigated whether this also applies in the case of anti-infective compounds. Ciprofloxacin and minocycline, antibiotics from two different classes which need to cross the IM to reach their target [38], were therefore tested and compared in both models. The results again revealed significant differences in P_{app} values, with both antibiotics permeating across the IM model to a greater extent than the mammalian comparator (Fig. 7A). The employment of bacteria-specific lipids in a permeation model of the IM (as well as in further bacterial envelope model development) is therefore deemed to be of great importance, in order to avoid underestimation of compound permeability - a problem which could be even further exacerbated when additional permeation barriers of the bacterial cell envelope (such as the OM) are taken into account.

In a further step, an additional antibiotic, PMB, was employed in conjunction with either ciprofloxacin or minocycline, in order to investigate the existence of functional similarity between the bacterial IM model and the Gram-negative bacterial inner membrane itself. PMB is known to interact in an electrostatic manner at *in cellulo* assay concentrations [39] with acidic PLs such as POPG and CL, as found in the Gram-negative bacterial inner membrane [40,41]; this interaction is followed by insertion into the membrane structure, pore formation and subsequent weakening of the membrane barrier function. In contrast, at similar PMB concentrations, no such interaction and disruption is observed with membranes containing overall electroneutral PLs like PC [40], as present in the mammalian comparator model. As a result of its permeabilizing effect on the Gram-negative inner membrane, PMB may be used clinically in a combination therapy approach together with other antibiotics such as the

currently employed minocycline [42,43], in order to provide enhanced cytoplasmic entry and target access. To determine whether this scenario was reflected in the current *in vitro* approach, both models were incubated with PMB in a relevant *in cellulo* assay concentration, as previously shown to affect the IM of *Escherichia coli* [40]. Ciprofloxacin or minocycline were then applied to the models, and compound permeation was again assessed. Both ciprofloxacin and minocycline showed significantly higher P_{app} values in the IM model following PMB treatment (Fig. 7B), whereas no significant difference in P_{app} was noted for either antibiotic in the mammalian comparator model as a result of incubation with PMB (Fig. 7B). The observed permeabilization of the IM model (and corresponding lack of effect in the mammalian comparator model) confirms a functional similarity of this structure to the Gram-negative bacterial inner membrane. This study therefore provides a clear example of the superior capacity of the bacterial IM model for evaluation of anti-infective permeation, further highlighting the importance of employing bacteria-specific lipids in model development.

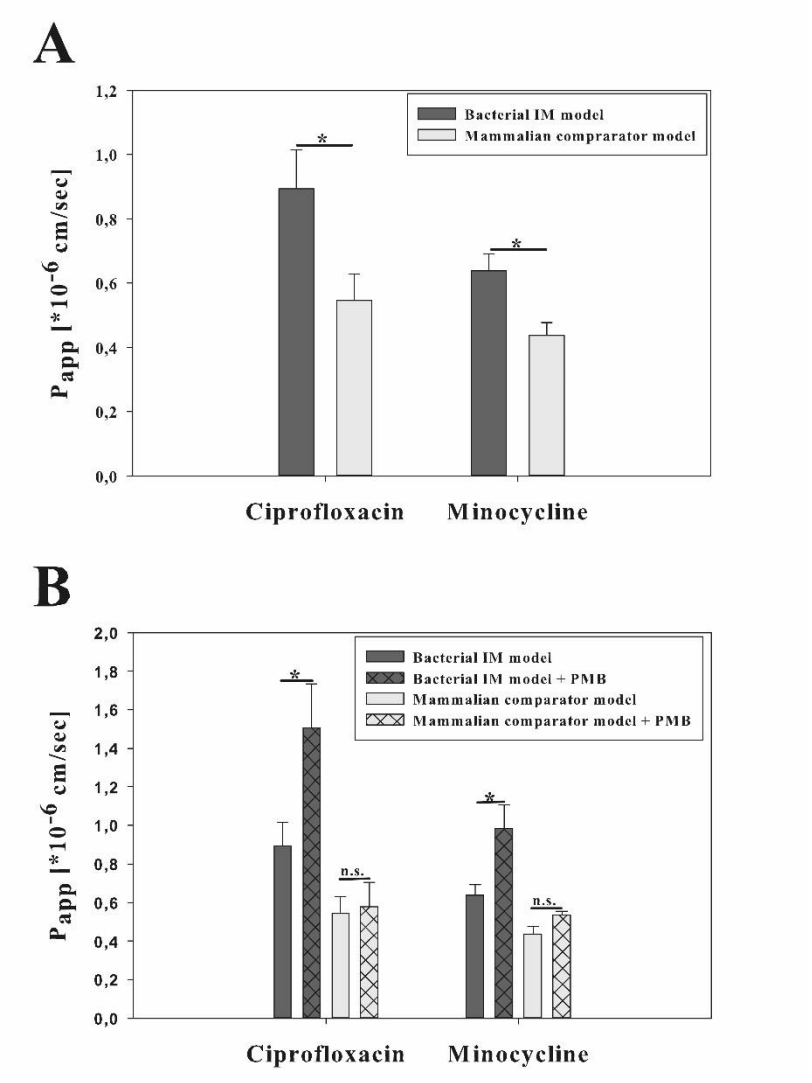

Fig. 7. Permeability experiment results of anti-infectives. P_{app} values of ciprofloxacin and minocycline in the bacterial IM and mammalian comparator model are shown (A), and are compared with P_{app} values following pre-incubation of both models with PMB (B). Values represent mean ± SE; n=6 from 2 individual experiments; *=P<0.05, n.s. = not significant.

3.4 Comparison of the IM model to an established vesicle-based assay

Following clear demonstration of the advantage and need for the bacterial IM model, the IM model permeation of an anti-infective-derived structure was investigated in a final, small scale exploratory study, to allow for clear comparison of data obtained with the current model to that derived from an established anti-infective permeation assay. In this respect, a hydroxyguanidine-functionalized fatty acid moiety derived from the muraymycin A-series of nucleoside antibiotics was chosen – this structure is proposed to account for the increased activity of the A-series congeners in comparison to other muraymycins, due to its ability to facilitate an increase in membrane permeability [44,45]. Recently, a simplified model system was employed to experimentally validate this proposed. In this respect, the hydroxyguanidine-functionalized fatty acid moiety, covalently linked to a fluorophore (AlexaFluor 488), was applied in a vesicle-based *in vitro* model (not entirely utilizing bacteria-relevant PL components) [23]. For comparison, a reference compound, lacking the hydroxyguanidine-functionalized fatty acid motif, was employed. The functionalized fatty acid was observed to permeate into lipid vesicles to a greater extent than the reference compound, assessed by evaluating the fluorescence intensity inside vesicles relative to background; furthermore, the functionalized fatty acid was seen to accumulate at the membrane interface right after the addition of the compound to the immobilized vesicles [23]. However, it could not be elucidated if this accumulation corresponded to a rapid permeation of the compound, due to insufficient assay sensitivity.

In the current work, as for the previous vesicle-based study, the permeability of the ω-hydroxyguanidinylated fatty acid conjugate was assessed in comparison to the reference compound composed of the fluorescent label and linker alone (see Supplementary Material Figure S6). Higher permeation rates as well as a significantly higher P_{app} value were found for the functionalized fatty acid as compared to the reference compound in the bacterial IM

model (Fig. 8), confirming the previous findings of the vesicle-based assay [23]. A further very notable result from the kinetically-resolved data as shown in Fig. 8A is the high permeated amount of the functionalized fatty acid conjugate at 0 h. This observation strongly suggests that the previously noted rapid accumulation effect does seem to correlate with immediate membrane permeation, followed by a second permeation phase. This two-phase model for the permeation of the functionalized fatty acid conjugate could only be derived from kinetically-resolved data as facilitated by use of the IM model, thus further highlighting the relevance of this new approach.

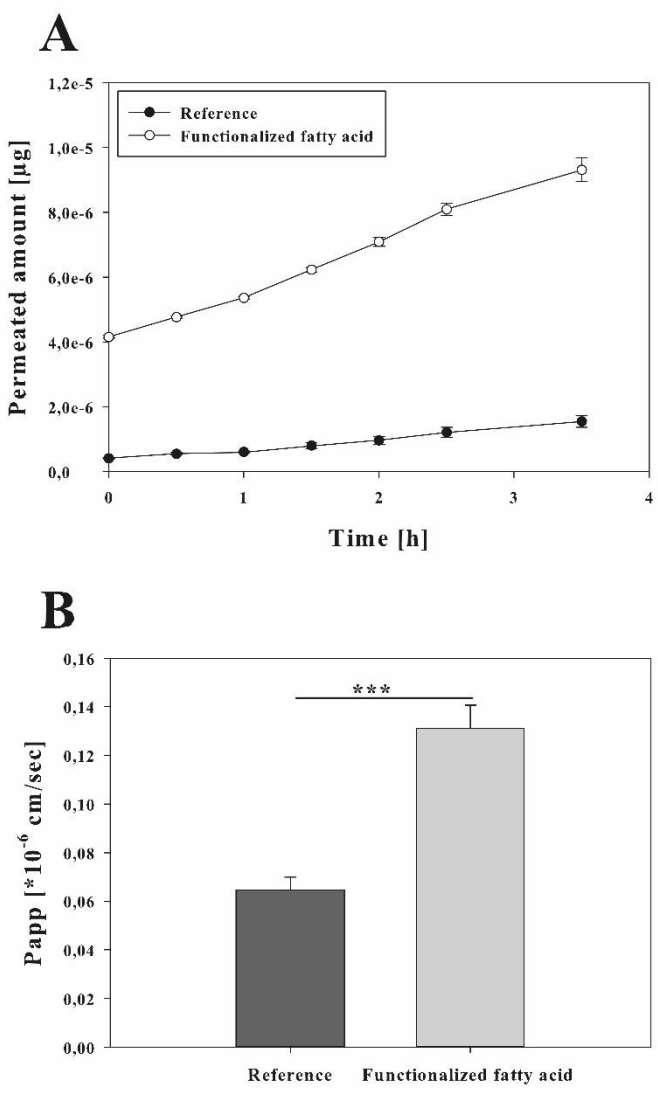

Fig. 8. Permeability experiment results of employed functionalized fatty acid moieties. Permeation rate and extent of the hydroxyguanidinylated fatty acid and reference compound (A), showing a permeability enhancing effect of the functionalized fatty acid moiety. The finding is also reflected in the calculated P_{app} values (B), additionally highlighting the advantage of the IM model for quantification of permeation processes and assessment of the permeation kinetics of tested compounds. Values represent mean ± SE; n=9 from 3 individual experiments; ***=P<0.001.

4. Conclusion

We herein report the successful development of a stable and robust *in vitro* permeation model of the Gram-negative bacterial IM, composed of bacteria-relevant PLs in a physiological ratio. Characterization of the IM model and its components from the molecular level to the macroscale, and comparison with an identically-produced model created from mammal-relevant PC indicated a number of PL-related model deviations. These deviations were ultimately shown to translate to significant differences in permeability of both model compounds as well as anti-infectives as a function of model PL composition. The ability of the novel IM model setup to provide quantitative data regarding the rate and extent of compound permeation was also demonstrated, facilitating a more accurate characterization of compound permeation as well as more information-rich evaluation of drug delivery approaches across the IM models. Future work focuses on the development of an OM model, in a further step towards creating a relevant permeation model of the complete Gram-negative bacterial cell envelope.

Acknowledgements

The authors acknowledge Christoph Pauly (Department of Material Science And Engineering, Chair of Functional Materials, Saarland University) for his assistance in the laser scanning interferometry analysis, and the Core Facility for Integrated Microscopy, Faculty of Health and Medical Sciences, University of Copenhagen for the assistance in taking the cryo-SEM images.

Funding

This research did not receive any specific grant from funding agencies in the public, commercial, or not-for-profit sectors.

References

[1] E.M. Wellington, A.B. Boxall, P. Cross, E.J. Feil, W.H. Gaze, P.M. Hawkey, A.S. Johnson-Rollings, D.L. Jones, N.M. Lee, W. Otten, C.M. Thomas, A.P. Williams, The role of the natural environment in the emergence of antibiotic resistance in gram-negative bacteria, Lancet Infect. Dis., 13 (2013) 155-165.

[2] M. McKenna, Antibiotic resistance: the last resort, Nature, 499 (2013) 394-396.

[3] F.C. Tenover, Mechanisms of antimicrobial resistance in bacteria, Am. J. Med., 119 (2006) 3-10.

[4] M. Thein, G. Sauer, N. Paramasivam, I. Grin, D. Linke, Efficient subfractionation of gram-negative bacteria for proteomics studies, J. Proteome Res., 9 (2010) 6135-6147.

[5] M.L. Nelson, Grier, M.C., Barbaro, S. E., and Ismail M. Y., Polyfunctional antibiotics affecting bacterial membrane dynamics, Anti-Infect. Agents Med. Chem., 8 (2009) 3-16.

[6] H.I. Zgurskaya, C.A. López, S. Gnanakaran, Permeability barrier of Gram-negative cell envelopes and approaches to bypass it, ACS Infect. Dis., 1 (2015) 512-522.

[7] T.J. Silhavy, D. Kahne, S. Walker, The bacterial cell envelope, Cold Spring Harb. Perspect. Biol., 2 (2010) a000414.

[8] F. Graef, S. Gordon, C.M. Lehr, Anti-infectives in drug delivery-overcoming the Gram-negative bacterial cell envelope, Curr. Top. Microbiol. Immunol., (2016) epub ahead of print 1-22.

[9] K. Takrouri, H.D. Cooper, A. Spaulding, P. Zucchi, B. Koleva, D.C. Cleary, W. Tear, P.J. Beuning, E.B. Hirsch, J.B. Aggen, Progress against Escherichia coli with the oxazolidinone class of antibacterials: Test case for a general approach to improving whole-cell Gram-negative activity, ACS Infect. Dis., 2 (2016) 405-426.

[10] J.M. Pages, C.E. James, M. Winterhalter, The porin and the permeating antibiotic: a selective diffusion barrier in Gram-negative bacteria, Nat. Rev. Microbiol., 6 (2008) 893-903.

[11] E.M. Nestorovich, C. Danelon, M. Winterhalter, S.M. Bezrukov, Designed to penetrate: time-resolved interaction of single antibiotic molecules with bacterial pores, Proc. Natl. Acad. Sci. U. S. A., 99 (2002) 9789-9794.

[12] J. van Weerd, M. Karperien, P. Jonkheijm, Supported lipid bilayers for the generation of dynamic cell-material interfaces, Adv. Healthcare. Mater., 4 (2015) 2743-2779.

[13] A.I. Kuzmenko, H. Wu, F.X. McCormack, Pulmonary collectins selectively permeabilize model bacterial membranes containing rough lipopolysaccharide, Biochemistry, 45 (2006) 2679-2685.

[14] L.A. Clifton, S.A. Holt, A.V. Hughes, E.L. Daulton, W. Arunmanee, F. Heinrich, S. Khalid, D. Jefferies, T.R. Charlton, J.R. Webster, C.J. Kinane, J.H. Lakey, An accurate in vitro model of the E. coli envelope, Angew. Chem., Int. Ed. Engl., 54 (2015) 11952-11955.

[15] D.I. Fernandez, A.P. Le Brun, T.H. Lee, P. Bansal, M.I. Aguilar, M. James, F. Separovic, Structural effects of the antimicrobial peptide maculatin 1.1 on supported lipid bilayers, Eur. Biophys. J., 42 (2013) 47-59.

[16] T. Mach, P. Neves, E. Spiga, H. Weingart, M. Winterhalter, P. Ruggerone, M. Ceccarelli, P. Gameiro, Facilitated permeation of antibiotics across membrane channels-interaction of the quinolone moxifloxacin with the OmpF channel, J. Am. Chem. Soc., 130 (2008) 13301-13309.

[17] M. Luckey, H. Nikaido, Specificity of diffusion channels produced by lambda phage receptor protein of Escherichia coli, Proc. Natl. Acad. Sci. U. S. A., 77 (1980) 167-171.

[18] J.L. Gornall, K.R. Mahendran, O.J. Pambos, L.J. Steinbock, O. Otto, C. Chimerel, M. Winterhalter, U.F. Keyser, Simple reconstitution of protein pores in nano lipid bilayers, Nano Lett., 11 (2011) 3334-3340.

[19] K. Lewis, Antibiotics: Recover the lost art of drug discovery, Nature, 485 (2012) 439-440.

[20] G.E. Flaten, A.B. Dhanikula, K. Luthman, M. Brandl, Drug permeability across a phospholipid vesicle based barrier: a novel approach for studying passive diffusion, Eur. J. Pharm. Sci., 27 (2006) 80-90.
[21] R.M. Epand, R.F. Epand, Bacterial membrane lipids in the action of antimicrobial agents, J. Pept. Sci., 17 (2011) 298-305.
[22] A.D. Bangham, M.M. Standish, J.C. Watkins, Diffusion of univalent ions across the lamellae of swollen phospholipids, J. Mol. Biol., 13 (1965) 238-252.
[23] O. Ries, C. Carnarius, C. Steinem, C. Ducho, Membrane-interacting properties of the functionalised fatty acid moiety of muraymycin antibiotics, Med. Chem. Comm., 6 (2015) 879-886.
[24] J.T. Davies, E.K. Rideal, Interfacial phenomena, Academic Press, New York, 1963.
[25] D. Marsh, Lateral pressure in membranes, Biochim. Biophys. Acta, 1286 (1996) 183-223.
[26] G.E. Flaten, H. Bunjes, K. Luthman, M. Brandl, Drug permeability across a phospholipid vesicle-based barrier 2. Characterization of barrier structure, storage stability and stability towards pH changes, Eur. J. Pharm. Sci., 28 (2006) 336-343.
[27] G.E. Flaten, M. Skar, K. Luthman, M. Brandl, Drug permeability across a phospholipid vesicle based barrier: 3. Characterization of drug-membrane interactions and the effect of agitation on the barrier integrity and on the permeability, Eur. J. Pharm. Sci., 30 (2007) 324-332.
[28] S.M. Fischer, G.E. Flaten, E. Hagesaether, G. Fricker, M. Brandl, In-vitro permeability of poorly water soluble drugs in the phospholipid vesicle-based permeation assay: the influence of nonionic surfactants, J. Pharm. Pharmacol., 63 (2011) 1022-1030.
[29] F. Leonard, E.M. Collnot, C.M. Lehr, A three-dimensional coculture of enterocytes, monocytes and dendritic cells to model inflamed intestinal mucosa in vitro, Mol. Pharm., 7 (2010) 2103-2119.
[30] C.I. Grainger, L.L. Greenwell, D.J. Lockley, G.P. Martin, B. Forbes, Culture of Calu-3 cells at the air interface provides a representative model of the airway epithelial barrier, Pharm. Res., 23 (2006) 1482-1490.
[31] S.P. Gantzsch, B. Kann, M. Ofer-Glaessgen, P. Loos, H. Berchtold, S. Balbach, T. Eichinger, C.M. Lehr, U.F. Schaefer, M. Windbergs, Characterization and evaluation of a modified PVPA barrier in comparison to Caco-2 cell monolayers for combined dissolution and permeation testing, J. Control. Release, 175 (2014) 79-86.
[32] A. Avdeef, Absorption and drug development: Solubility, permeability and charge state, Wiley, Hoboken, NJ, USA, 2012.
[33] A. Malkia, L. Murtomaki, A. Urtti, K. Kontturi, Drug permeation in biomembranes: in vitro and in silico prediction and influence of physicochemical properties, Eur. J. Pharm. Sci., 23 (2004) 13-47.
[34] A.M. Marino, M. Yarde, H. Patel, S. Chong, P.V. Balimane, Validation of the 96 well Caco-2 cell culture model for high throughput permeability assessment of discovery compounds, Int. J. Pharm., 297 (2005) 235-241.
[35] M. Kansy, F. Senner, K. Gubernator, Physicochemical high throughput screening: parallel artificial membrane permeation assay in the description of passive absorption processes, J. Med. Chem., 41 (1998) 1007-1010.
[36] A. Avdeef, The rise of PAMPA, Expert Opin. Drug Metab. Toxicol., 1 (2005) 325-342.
[37] C. Zhu, L. Jiang, T.M. Chen, K.K. Hwang, A comparative study of artificial membrane permeability assay for high throughput profiling of drug absorption potential, Eur. J. Med. Chem., 37 (2002) 399-407.
[38] R.E.W. Hancock, A. Bell, Antibiotic uptake into Gram-negative bacteria, in: G.G. Jackson, H.D. Schlumberger, H.J. Zeiler (Eds.), Perspectives in anti-infective therapy, Wiesbaden 1989, pp 11-29.

[39] R. Daugelavicius, E. Bakiene, D.H. Bamford, Stages of polymyxin B interaction with the Escherichia coli cell envelope, Antimicrob. Agents Chemother., 44 (2000) 2969-2978.
[40] D.R. Storm, K.S. Rosenthal, P.E. Swanson, Polymyxin and related peptide antibiotics, Annu. Rev. Biochem., 46 (1977) 723-763.
[41] M. Teuber, J. Bader, Action of polymyxin B on bacterial membranes. Binding capacities for polymyxin B of inner and outer membranes isolated from Salmonella typhimurium G30, Arch. Microbiol., 109 (1976) 51-58.
[42] Y. Zhang, F. Chen, E. Sun, R. Ma, C. Qu, L. Ma, In vitro antibacterial activity of combinations of fosfomycin, minocycline and polymyxin B on pan-drug-resistant Acinetobacter baumannii, Exp. Ther. Med., 5 (2013) 1737-1739.
[43] D.R. Bowers, H. Cao, J. Zhou, K.R. Ledesma, D. Sun, O. Lomovskaya, V.H. Tam, Assessment of minocycline and polymyxin B combination against Acinetobacter baumannii, Antimicrob. Agents. Chemother., 59 (2015) 2720-2725.
[44] L.A. McDonald, L.R. Barbieri, G.T. Carter, E. Lenoy, J. Lotvin, P.J. Petersen, M.M. Siegel, G. Singh, R.T. Williamson, Structures of the muraymycins, novel peptidoglycan biosynthesis inhibitors, J. Am. Chem. Soc., 124 (2002) 10260-10261.
[45] D. Wiegmann, S. Koppermann, M. Wirth, G. Niro, K. Leyerer, C. Ducho, Muraymycin nucleoside-peptide antibiotics: uridine-derived natural products as lead structures for the development of novel antibacterial agents, Beilstein J. Org. Chem., 12 (2016) 769-795.